

Self-Starting Switchable Multifunctional Solitons Fiber Laser

Renlai Zhou,* Hui Hu, Bo Guo, Qian Li, Hong Yan Fu, and K. Nakkeeran

Modern solitons fiber lasers systems sought for imaging, micromachining, metrology, spectroscopy, and sensing applications, require multifunctional light sources with fully controlled switching features to avail the necessary optical signal. Existing single cavity fiber laser systems have limitations on the generation of multistate solitons due to the intrinsic dispersion, nonlinearity, filtering, gain, and loss. Herein, for the very first time, a compact multifunctional solitons fiber laser controlled by the 3D maneuvering of the polarization beam splitter (PBS) to select the appropriate polarization state for various mode-locked operations is demonstrated. For single soliton state operation, conventional solitons (CSs), quasi-coherent noise-like pulses (QC-NLPs) and harmonic mode-locking (HML) are achieved independently, and these different states can be easily and efficiently switched by steering the PBS position. Versatile hybrid dual-wavelength mode-locked operations (2-CSs states, 1-CS state and 1-QC-NLP state, and 2-QC-NLPs states) are additional functionalities achievable when the PBS position is steered to suitable positions. The hybrid dual-wavelength mode-locked operation has excellent long-term stability even functioning at maximum output power. It is envisaged that the proposed work provides a compact switchable multifunctional solitons fiber laser system that can be potentially applied in optics signal processing, micromachining, spectroscopy, and optical sensing, etc.

for material processing,^[1] optical communications,^[2] microwave photonics,^[3] biomedical imaging,^[4] and spectroscopy.^[5] Passively mode-locked fiber lasers that can generate optical pulses with different shapes and durations from picosecond (ps) to tens of femtosecond (fs) are getting popular for ultrashort pulses generation, solitons dynamics research and related applications. In the optical fiber laser system, dispersion, nonlinearity, filtering, polarization, gain, and loss play a critical role in the formation of the ultrashort pulses. When the net laser cavity dispersion aggregates to anomalous, near-zero, or normal regime, respectively, conventional solitons (CSs),^[6] stretched pulses (SPs),^[7] or dissipative solitons^[8] can be mode-locked in the fiber laser system. In contrast, lasing of noise-like pulses (NLPs) is a special mode-locking operation, which possesses longer pulse duration, various pulse patterns, higher pulse energy, and smooth broadband spectrum. Owing to these distinct features, NLPs are becoming a hot research topic in the study of fiber lasers, such as real-time dynamics of NLPs

1. Introduction

With features like high peak power, low thermal effect, high transfer efficiency etc., ultrashort pulse lasers are widely used


formation,^[9] and quasi-coherent NLPs (QC-NLPs).^[10] Hitherto diversiform soliton pulses can be obtained through different cavity configurations, and their dynamics and applications have been extensively investigated. However, with the rapid

R. Zhou, H. Hu, B. Guo
Key Laboratory of In-Fiber Integrated Optics
Ministry Education of China
College of Physics and Optoelectronic Engineering
Harbin Engineering University
Harbin 150001, China
E-mail: zrlhit@126.com

Q. Li
School of Electronic and Computer Engineering
Peking University
Shenzhen 518055, China

H. Y. Fu
Tsinghua Shenzhen International Graduate School and Tsinghua-Berkeley
Shenzhen Institute
Tsinghua University
Shenzhen 518055, China

K. Nakkeeran
School of Engineering
Fraser Noble Building
University of Aberdeen
Aberdeen AB24 3UE, UK

 The ORCID identification number(s) for the author(s) of this article can be found under <https://doi.org/10.1002/adpr.202100348>.

© 2022 The Authors. Advanced Photonics Research published by Wiley-VCH GmbH. This is an open access article under the terms of the Creative Commons Attribution License, which permits use, distribution and reproduction in any medium, provided the original work is properly cited.

DOI: 10.1002/adpr.202100348

development of modern medicine and industry, many applications, including advanced micromachining,^[11,12] imaging,^[13,14] and metrology,^[15,16] increasingly rely on switchable multifunctional soliton fiber lasers, where reproducible and controllable features are particularly required. Limited by the complex dynamics of dispersion, nonlinearity, filtering, polarization, gain, and loss in the lasing cavity, little attention has been paid to the multistate soliton generation from a single oscillator cavity and the practical applications of which need to be further exploited. In particular, Tang et al.^[17] theoretically and experimentally demonstrated the two different types of soliton-shaping that could compete and coexist in a laser cavity with near-zero dispersion. Coexistence of higher order harmonic soliton molecule and NLPs was experimentally demonstrated in a mode-locked fiber laser.^[18] Bidirectional mode-locked fiber lasers that can independently generate solitons in one/two cavities with different cavity lengths and/or net-cavity dispersions were designed and investigated.^[19–24] Dual-wavelength mode-locked fiber lasers based on a programmable spectral filter were reported, where the frequency spacing between the dual wavelengths can be tuned by balancing the gain competition between the two different lasing wavelengths.^[25,26] Results reported so far in the literature on the multistate solitons generation in fiber lasers, mainly focused on the tunability of the peak wavelength and frequency spacing between the dual-wavelength mode-locking, and the dual-type solitons generation in complex multi-cavity or polarization-multiplexing fiber lasers. Whether the multistate soliton generation, namely CSs, NLPs, dual-wavelength mode-locking, and harmonics mode-locking (HML), feasible in a single laser cavity? Also, how to effectively switch between all possible stable and reliable multistate mode-locking operations in the cavity? It is crucial to focus on the investigations of these important multifunctionalities of the soliton fiber laser.

To generate ultrashort pulses in fiber lasers, quite commonly, nonlinear polarization evolution (NPE) is used as an effective method,^[10,27] which involves efficient energy transfer, high modulation depth, and rapid saturation absorption. In conventional NPE mode-locked lasers, several half-wave plates (HWP), and quarter-wave plates (QWP) are included in the cavity to adjust the polarization state of the light signal in free space. Shang et al. reported a simple NPE mode-locked erbium-doped fiber (EDF) laser that replaced all the bulk-optics HWP and QWP devices with a single polarization beam splitter (PBS).^[28] However, in that setup, it was difficult to realize the mode-locking buildup only through the rotation of the PBS in the cavity, and the mode-locking operation was very sensitive to perturbations such as slight vibration of the fiber or minor disturbance to the platform. To overcome these constraints and difficulties, we introduced an in-line polarization controller (PC) in the lasing cavity, which generated highly stable QC-NLPs with a first-order whole spectral coherence of ~ 0.408 .^[10] Using the birefringent filtering effect of the optical fibers, the peak wavelength of the QC-NLPs could be fine-tuned through 3D maneuvering of the PBS position, which in addition provided the polarization control and state selection of the intracavity light signal. With these features available in our proposed fiber laser, there emerges an open question whether it would be possible to achieve different soliton states in a compact self-starting switchable mode-locked fiber laser through 3D maneuvering of the PBS position?

In this article, via 3D manipulation of the PBS position to select the polarization state of the light signal in the cavity, for the very first time, we experimentally demonstrate how different soliton states between CSs, QC-NLPs, versatile hybrid dual-wavelength mode-locking, and HML can be effectively switched in a compact simplified NPE fiber laser. The output characteristics of the multistate solitons formation are investigated in detail, especially the reversibly switching between the CSs, QC-NLPs, and versatile hybrid dual-wavelength mode-locking operations. This research work not only demonstrates the working principle of a self-starting switchable multifunctional solitons fiber laser for potential applications, but also introduces a new equipment to explore the multifunctional operations and nonlinear dynamics of ultrafast fiber lasers.

2. Experimental Section

The experimental setup of the proposed mode-locked fiber laser is shown in **Figure 1a**. Different from the traditional NPE mode-locked fiber lasers, the HWP and QWP were all replaced by a PBS in the cavity. To fine control the position of the PBS, an assembly of a precise optical adjustment bracket and a rotary platform were devised to control the angle of pitch and regulate the rotation angle, which has $<1\ \mu\text{m}$ high sensitivity and $<5\ \mu\text{m}$ movement precision. A $\approx 1.05\ \text{m}$ long EDF (Nufern) was used as the gain fiber in the cavity that was pumped by a 976 nm laser diode (LD) through a 980/1550 nm wavelength-division multiplexer (WDM). The splice-loss between LD and WDM is $\approx 10\%$, and the maximum possible pump power from the WDM is $\approx 540\ \text{mW}$. An in-line PC was employed for filtering the intracavity polarization state to improve the lasing and stabilization of the mode-locking operation. The light signal oscillating in the cavity was confined to maintain unidirectional propagation using a polarization-insensitive isolator (PI-ISO). The total cavity length was $\approx 11.64\ \text{m}$, and $-0.338\ \text{ps}^2$ net-cavity dispersion indicates the cavity operated in the anomalous dispersion regime. The output laser was coupled out from a three-port 3-dB fiber coupler, where one output port was connected to an optical spectrum analyzer (AQ6370D, Yokogawa) with a resolution of 0.02 nm, while the other was connected to a real-time oscilloscope (DPO-75902SX, Tektronix) with a $>25\ \text{GHz}$ bandwidth InGaAs photodiode detector (UPD-15-IR2-FC). The frequency of the output pulses was monitored by a radio-frequency (RF) signal analyzer (N9030B, Agilent) with a bandwidth from 3 Hz to 50 GHz. The intensity autocorrelation (AC) trace of the train of mode-locked pulses was measured by a commercial autocorrelator (FR-103XL, Femtochrome).

In NPE fiber lasers, conventionally the light signal is decomposed into two components by the unadjusted PBS, and these light signals possess fixed orthogonal polarization states. But the PBS can be 3D maneuvered along its vertical z -axis for any required changes of the polarization state of the light signal that would determine the amount of transmission/reflection. The angle between the reflected light and y -axis, θ as pictorially illustrated in the dashed box inset in **Figure 1a** can be used for the calculation of the transmission/reflection coefficient. For conventional NPE laser ($\theta = 0$), the output components of

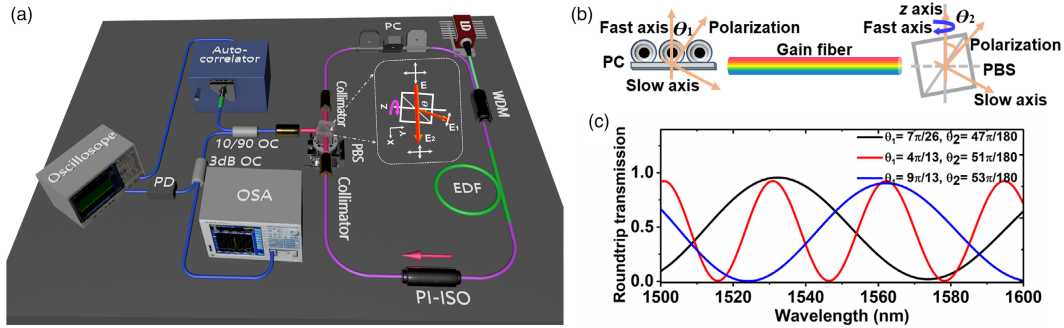


Figure 1. a) Schematic diagram of the proposed mode-locked fiber laser, OSA: optical spectrum analyzer; WDM: wavelength-division multiplexer; OC: optical coupler. b) Three main polarization state blocks of the NPE laser. c) Calculated roundtrip transmission curves with different polarization angles θ_1 and θ_2 .

PBS can be expressed as $\begin{bmatrix} E_1 \\ E_2 \end{bmatrix} = \begin{bmatrix} 1 & 0 \\ 0 & 1 \end{bmatrix} \begin{bmatrix} E_x \\ E_y \end{bmatrix}$. When the PBS is 3D maneuvered along its vertical z-axis, the output components of PBS were changed as $\begin{bmatrix} E'_1 \\ E'_2 \end{bmatrix} = \begin{bmatrix} r_x(\theta) & 0 \\ t_x(\theta) & 1 \end{bmatrix} \begin{bmatrix} E_x \\ E_y \end{bmatrix}$. Here, $r_x(\theta)$ and $t_x(\theta)$ are the reflection and transmission coefficient of E_x , respectively. In the lasing cavity, the polarization state of the light signal arriving at the PBS can be oriented either with the polarization state of the (decomposed) transmitted or reflected light, which functions as a polarization analyzer. For a better understanding of the different soliton states mode-locking mechanism of the proposed fiber laser, we expressed the NPE laser as three main polarization state blocks as shown in Figure 1b. By considering θ_1 as the angle between the fast axis of the gain fiber and the polarization state of the light signal set by the PC and θ_2 as the angle between the fast axis of gain fiber and the 3D maneuvered PBS polarization state, the transmission function can be expressed as follows.^[29]

$$T = \cos^2\theta_1 \cos^2\theta_2 + \sin^2\theta_1 \sin^2\theta_2 + \frac{1}{2} \sin(2\theta_1) \sin(2\theta_2) \cos(\Delta\varphi_L + \Delta\varphi_{NL}) \quad (1)$$

where $\Delta\varphi_L = 2\pi L(n_x - n_y)/\lambda$, $\Delta\varphi_{NL} = 2\pi n_2 PL \cos(2\theta_1)/\lambda A_{\text{eff}}$, $B_m = |n_x - n_y|$. $\Delta\varphi_L$ and $\Delta\varphi_{NL}$ are the linear and nonlinear phase delays in the cavity. B_m is the strength of modal birefringence, determined by the refractive indices of the fast axis n_x and slow axis n_y of the optical fiber. P is the peak power of the input pulse. L is the birefringence length of the fiber, n_2 is the nonlinear refractive index. λ is the operating wavelength, and A_{eff} is the effective core area. Calculated roundtrip transmission curves for various θ_1 and θ_2 are shown in Figure 1c. These characteristics show the possibilities for the light signal oscillating inside the cavity can be periodically modulated with features to have different transmission wavelength peaks and frequency spacing. This is because of the birefringence filtering effect of the fiber laser cavity, which is assisted by the polarization states provided through 3D maneuvering of the PBS position and adjustments of the PC orientation. Thus, the proposed NPE fiber laser can be operated in different single-wavelengths or dual-wavelengths. In the following section, we report the details of how the proposed

NPE fiber laser can be operated for different mode-locked soliton states.

3. Results and Discussions

3.1. Soliton and Quasi-Coherent Noise-like Pulses

CSs mode-locked state was achieved in the proposed fiber laser by steering the PBS position to $\approx 2^\circ$ clockwise and adjusting the PC orientation to get appropriate cavity loss. The self-starting threshold for this CSs state operation was ≈ 180 mW, i.e., stable (multi-pulse) CSs mode-locking was established when the pump power was increased directly to 180 mW. Using the cavity hysteresis, single-pulse CSs operation was obtained by gradually reducing the pump power to 135 mW, and the single-pulse state could be maintained for the pump power range of 45–135 mW. Mode-locking operation was lost when the pump power was reduced below 45 mW. Output characteristics of the CSs operation are exhibited in Figure 2. Measured 3-dB spectral bandwidth was 6.733 nm with a central wavelength of 1533.654 nm, which was consistent with the wavelength of the continuous wave (CW). Interestingly, asymmetric sidebands were observed in the spectrum, and the intensity of longer wavelength sidebands was higher than that of shorter wavelength sidebands. This feature could be due to the soliton Raman self-frequency shift, and in that the longer wavelength sidebands (Stoke's shift) are always enhanced compared to the shorter wavelength sidebands (anti-Stoke's shift), which leads to the generation of asymmetric sidebands in the spectrum.^[30] In addition, the birefringent filtering effect of the fiber laser cavity can also cause the intensity asymmetry in the spectral sidebands.^[29] If the initial projection angle θ_1 of the light signal locates in between $\frac{\pi}{4} < \theta_1 < \frac{\pi}{2}$, then the nonlinear phase delay $\Delta\varphi_{NL}$ will be negative. As a consequence, the loss experienced by the shorter wavelength sidebands will be higher than that of the longer wavelength sidebands, and hence the asymmetric sidebands are observed in the spectrum.

The oscilloscope trace is depicted in Figure 2b, where the time duration between two adjacent pulses is ≈ 56.95 ns, which corresponds to the roundtrip time of the laser cavity. The screenshot in the inset of Figure 2b shows the stable output pulse train. The RF spectrum of the soliton pulse train is presented

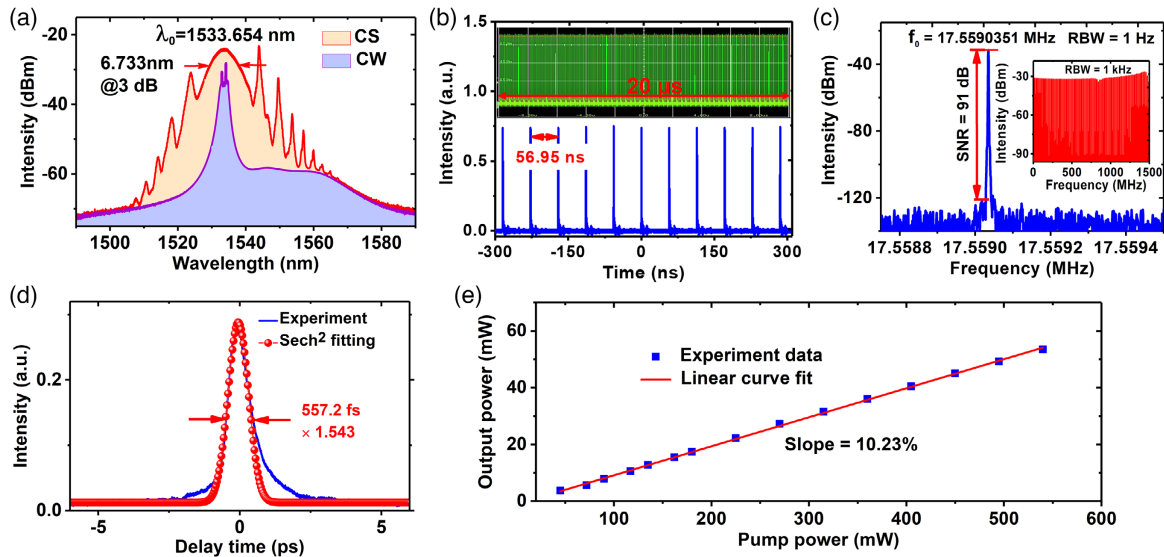


Figure 2. Output characteristics of CSs operation with PBS position at 2° : a) output spectra, b) oscilloscope trace, c) RF spectra, d) intensity AC trace, e) output power versus pump power.

in Figure 2c. The measured pulse repetition rate of 17.5590351 MHz was consistent with the fundamental repetition rate of the cavity. In the RF spectrum, a signal-to-noise ratio (SNR) higher than 90 dB with a 1-Hz resolution bandwidth (RBW) indicates that the mode-locking operated in a stable regime. A wideband RF spectrum up to 1500 MHz is shown as an inset in Figure 2c, and this also further confirmed the stable mode-locked operation of the fiber laser. The intensity AC trace is displayed in Figure 2d. Full width half maximum (FWHM) of pulse duration was ≈ 557.2 fs, which was calculated through a sech^2 profile fit for the measured pulse. Time-bandwidth product (TBP) was calculated as ≈ 0.466 , indicating that the output pulses

were slightly chirped and widened. The average output power increased linearly with the pump power, as shown in Figure 2e, which had a slope efficiency of 10.23%. Maximum average output power of 44.6 mW was achieved at an available pump power of 540 mW, and no saturation was observed within the available pump power range as shown in Figure 2e.

Further steering the PBS position to 3.2° clockwise, QC-NLPs operation was achieved with a suitable orientation of the PC, which was already reported.^[10] Compared with the CSs spectrum, the peak wavelength of QC-NLPs was shifted to 1530.847 nm with a 3-dB spectral bandwidth of 4.162 nm, as shown in Figure 3a. Quite contrast to the smooth spectrum of

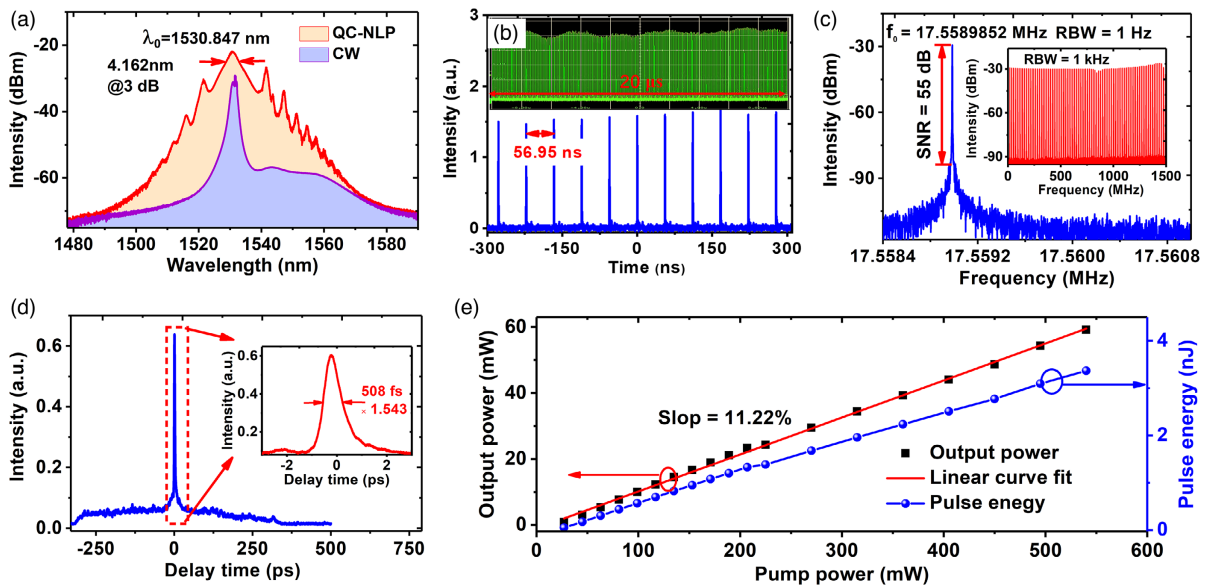


Figure 3. Output characteristics of QC-NLPs operation with PBS position at 3.2° : a) output spectra, b) oscilloscope trace, c) RF spectra, d) intensity AC trace, e) output power and energy versus pump power.

conventional NLPs, Kelly sidebands were observed in the spectrum of QC-NLPs, which highly improved first-order phase coherence for the NLPs. The bottom of Figure 3b shows the pulse train in the ns time scale that has a time gap of ≈ 56.95 ns between consecutive pulses. The top of Figure 3b shows the oscilloscope trace of NLPs in μ s time scale, which indicates the fluctuation in single pulse amplitude for this mode-locked state. The corresponding RF spectrum is depicted in Figure 3c. The pulse repetition rate was 17.5589852 MHz with a 1-Hz RBW, and the SNR was 55 dB at the fundamental frequency, implying the stability of the QC-NLPs operation is not as good as CSs operation. Up to 1500 MHz wideband RF spectrum is also presented in the inset of Figure 3c, and in that no envelope modulation was observed in the spectrum. The intensity AC trace of QC-NLP was measured and presented in Figure 3d, which shows a typical NLP feature of narrow coherent pulse profile (≈ 508 fs) on a wide shoulder. The intensity ratio between coherent peak and wide shoulder was ≈ 12 , which confirms the dominant role played by the coherent soliton part in the NLPs.

Measured average output power and single pulse energy of QC-NLPs as the function of pump power are shown in Figure 3e. The output power increased linearly with the pump power with a slope efficiency of 11.22%, and the maximum output power achievable was 59.2 mW. No saturation limit of the corresponding single pulse energy was observed up to the available pump power as shown in Figure 3e, and the highest single pulse energy of 3.37 nJ was achieved for the supplied pump power of 540 mW.

Based on the experimental results reported and discussed so far about the CSs (Figure 2) and QC-NLPs (Figure 3) regime of operations, we confirmed that the proposed NPE fiber laser can be operated in any of these two types of mode-locked soliton states, simply by 3D maneuvering of the PBS to appropriate positions. For CSs mode-locked operation, PBS position to be steered about 2.6° clockwise and with a pump power of 180 mW. With this CSs mode-locked operation in place by finely steering the PBS position from 2.6° to 3.2° , the CSs state was switched smoothly to QC-NLPs state. Correspondingly, the output spectrum switched from CSs state (purple curve) to QC-NLPs state (red curve) as shown in Figure 4a. When the PBS position was steered from 3.2° back to 2.6° , the mode-locked lasing operation reverse switched from QC-NLPs state to CSs state (blue curve in Figure 4a). Note that the locations of the Kelly sidebands in the direct (purple curve) and reverse switched (blue curve) CSs spectra are different, but the peak wavelength was retained.

Thus, the CSs and QC-NLPs states in the cavity could be switched either way by controlling the PBS position.

In contrast, the switching between the CSs and QC-NLPs mode-locked state could also be achieved by varying the pump power while maintaining the PBS position fixed at 4.5° clockwise. Figure 4b displays the measured output mode-locked spectra for different pump powers. The CSs state was switched to QC-NLPs state when the pump power was increased from 135 to 225 mW. The intensity of the Kelly sidebands got diminished when the mode-locked operation switched from CSs state to QC-NLPs state, but the spectral locations of the Kelly sidebands' spikes were retained. Further increase in the pump power increased the output spectral intensity, while the spectral bandwidth and profile of the QC-NLPs were almost unaltered.

3.2. Hybrid Dual-Wavelength Mode-Locking Operation

Dual-wavelength mode-locking is feasible in the fiber laser cavity as characterized by the transmission curve in Figure 1c. This could be achieved by suitably selecting the polarization state in the PBS that allows the birefringence filtering effect of the cavity to mode-lock multiple pulses with different wavelengths. Experimentally, dual-wavelength mode-locking operation was achieved by steering the PBS position to 6.2° clockwise. Also, this type of mode-locking was self-started when the pump power was raised to 135 mW. Once lasing self-started, dual-wavelength mode-locking operation was sustained in the cavity with pump power reduced up to 27 mW, below which it got unlocked. Figure 5a depicts the spectra corresponding to CW and dual-wavelength mode-locking. In the purple curve CW spectrum, three wavelength peaks of 1535.65, 1543.93, and 1564.47 nm were observed. Red curve dual-wavelength mode-locking spectrum shows the wavelengths peaks at 1535.652 nm (S2) and 1564.47 nm (S1), with a 3-dB spectral bandwidth of 6.61 nm and 4.551 nm, respectively. Pulse train and RF spectrum with 1-Hz RBW are shown in Figure 5b,c. Two independent pulse sequences are observed in the pulse train, which are depicted in both the ns (bottom) and μ s (top) scaled oscilloscope traces in Figure 5b. Slightly different repetition rates for the dual-colored pulses were observed as shown in Figure 5c, with a difference of ≈ 1.0588 kHz. This difference was caused by the different roundtrip group delays for different wavelengths in the dispersive fiber cavity. An oscilloscope was synchronized to screen-lock either one of the pulse trains, while the other pulse train run over it arbitrarily. SNRs of the dual-colored pulses were

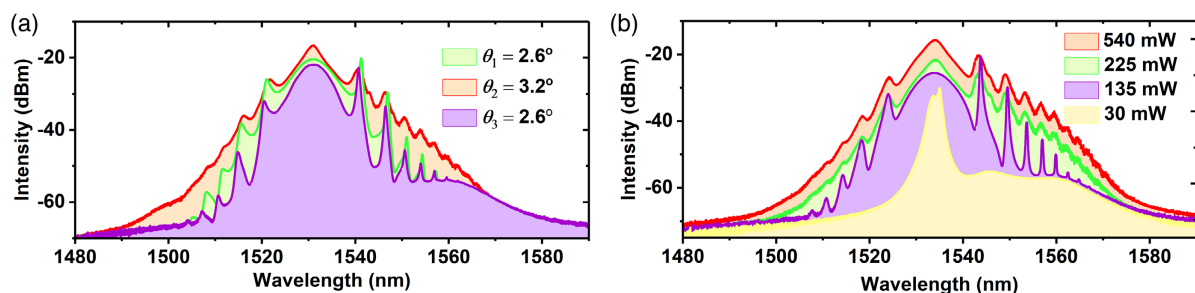


Figure 4. Switching of spectrum between CSs and QC-NLPs mode-locked states by varying: a) PBS position, b) pump power and PBS at 4.5° .

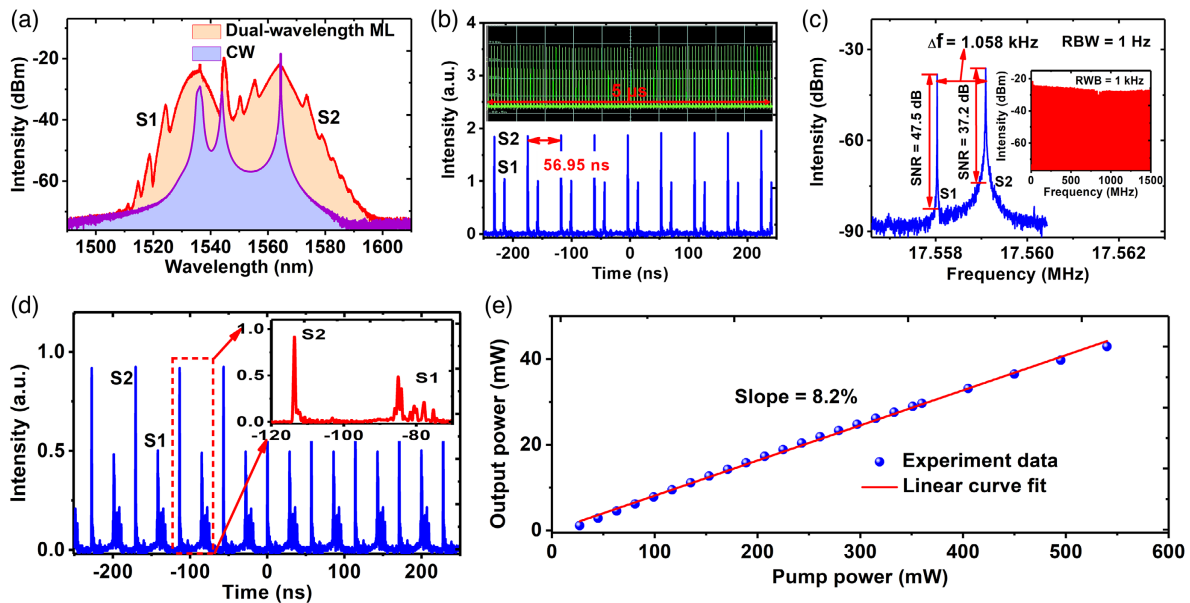


Figure 5. Dual-wavelength mode-locking operation with PBS position at 6.2° : a) output spectra of CW and mode-locking, b) oscilloscope trace at the pump power 135 mW, c) RF spectra, d) oscilloscope trace at the pump power 540 mW, e) output power versus pump power.

41.5 and 26.6 dB, and wideband RF spectrum up to a frequency of 1500 MHz manifest the stable operation of the dual-wavelength mode-locking. Beyond the pump power of 207 mW, one of the pulse-trains began to split, while the other maintained the single-pulse state. Figure 5d depicts the output pulse train for a pump power of 540 mW. Note that one pulse sequence had split into a multi-pulse state, while the other one was still a stable single-pulse state. Zoomed-in temporal pulse shown in the inset of Figure 5d indicates that one pulse transformed to an eight-peaked pulse. For the CSs operation in the net anomalous dispersion regime, the single laser pulse can be split into a random multi-pulse state when the pump power exceeds a certain value. Nevertheless, the NLPs can sustain stable single-pulse state operation at higher pump power. Hence, the dual-colored pulses lasing operation could have mode-locked two different types of solitons states, with an NLPs state, and another CSs state. The average output power of the dual-colored pulses increased linearly with the pump power with a slope efficiency of 8.2%, and the maximum obtained output power was 43.2 mW as presented in Figure 5e. Owing to partially overlapping output spectra of the dual-colored pulses, it was too difficult to precisely evaluate the individual power of the two spectra.

To investigate the output characteristics of this type of novel dual-wavelength mode-locking operation at a supplied pump power of 540 mW, the output signal spectra were manually separated by an optical tunable filter (TF-350, Santec) that has the facility to tune both the peak wavelengths and passband bandwidths. Separated output spectra with 50 nm bandwidth are shown in Figure 6a, in which the shorter (S2) and longer (S1) spectra are shown as red and purple curves, respectively. The filtered output pulse trains and RF spectra are depicted in Figure 6b,c. Temporal domain Figure 6b shows that the S1 and S2 pulse-trains were, respectively, single-pulsed and

multi-pulsed states. Higher SNR for S2 compared to S1 indicates the stability of the S2 operation was better than the S1 operation. To investigate the intensity AC trace of the dual-colored signal, the filtered mode-locked pulses were independently amplified through an EDFA and monitored by a commercial autocorrelator. For S1, a typical double-scaled structure made of a narrow pulse (≈ 574.5 fs) upon a wide pedestal was observed as shown in Figure 6d, where the intensity of the coherent pulse peak was much higher than the pedestal (intensity ratio ≈ 13), that could be categorized as QC-NLPs. For S2, the intensity AC trace indicates CSs mode-locking operation, where the FWHM pulse width was ≈ 520.3 fs, and the TBP was 0.412, as shown in Figure 6e. Thus, we confirmed this hybrid dual-wavelength mode-locking operation was comprised of QC-NLPs and CSs states. This is the first-time ever report of such a novel phenomenon observed in a single cavity laser.

To investigate the long-term stability of the hybrid dual-wavelength mode-locking operation of the proposed NPE fiber laser, the intensity spectrum was monitored with the setup kept operational in an open lab environment at room temperature. Results were periodically recorded at an interval of 1 min by the OSA for 150 min, and depicted in Figure 7a. The colored-contour plot represents the intensity distributions in the spectrum over time. Peak wavelengths, sidebands, and bandwidths showed high reliability over the entire observation period, indicating the stable operation of the hybrid dual-wavelength mode-locked state. In addition, both the separated pulse trains were monitored in the time domain for 150 min, and the results showed excellent long-term stability. Reliability and long-term stability of the repetition rate difference of the dual-colored pulses were examined by a frequency counter during the entire observation period. The beat frequency between the dual-colored pulses was recorded and presented in Figure 7b. Root-mean-square (RMS) and peak–peak

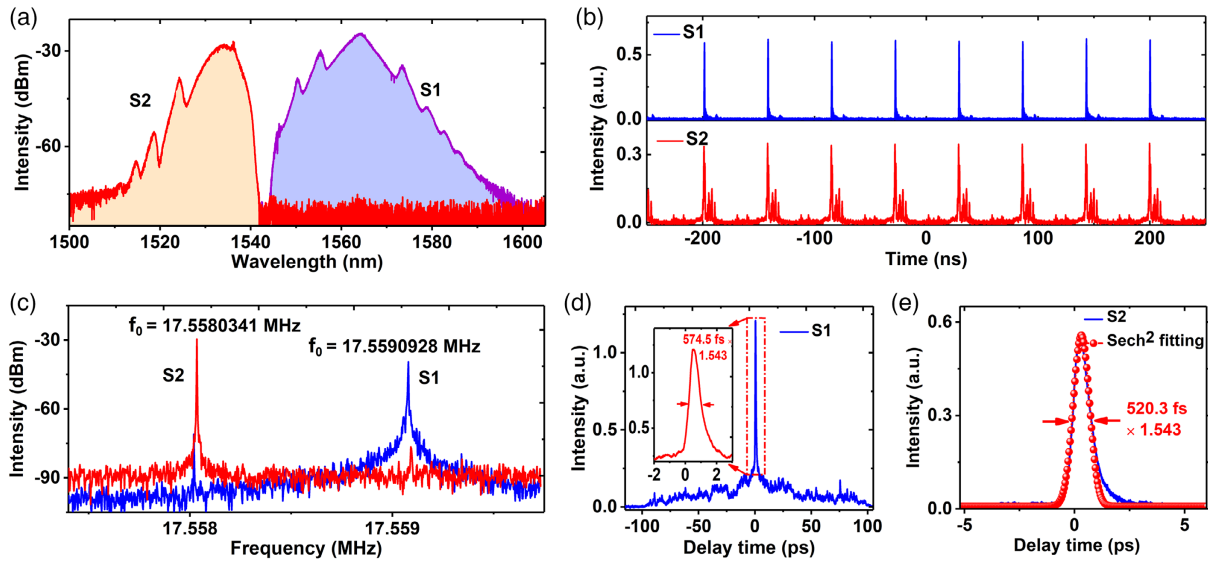


Figure 6. Filtered dual-colored mode-locked signal: a) output spectra, b) oscilloscope traces, c) RF spectra, and d,e) intensity AC traces of S1 and S2.

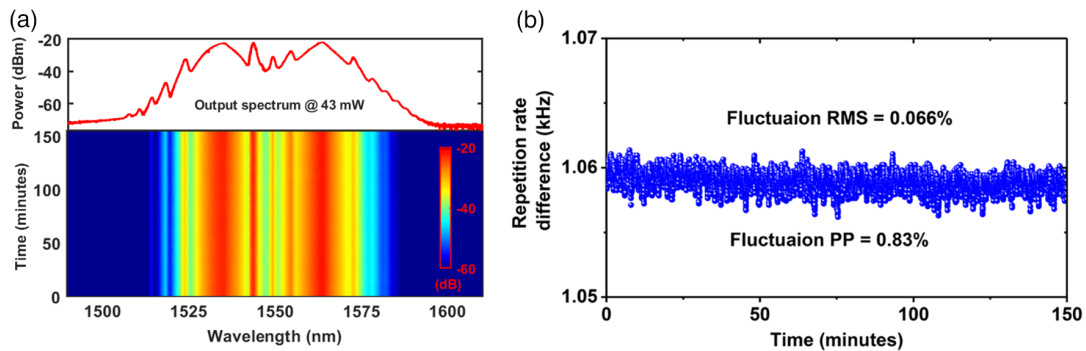


Figure 7. a) Long-term stability of the hybrid dual-wavelength mode-locking operation; b) observation of the stability of the repetition rate difference between the dual-colored pulse-trains.

(PP) fluctuations in the repetition rate difference were calculated as 0.066% and 0.83%, respectively, which again exhibit excellent stability.

In the proposed mode-locked fiber laser, by providing appropriate polarization axis bias to the oscillating light signal, simply through the 3D maneuvering of the PBS position, the interplay dynamics of the intracavity loss and birefringence filtering effect can mode-lock various different stable soliton states with single- and/or multi-pulse. Yet another feature in this fiber laser could be the tunability of the dual-colored pulses wavelengths spacing. **Figure 8a** depicts the output spectra of the dual-wavelength mode-locked state with wavelengths spacing tuned from 30.488 to 28.7204 nm by steering the PBS position from 7° to 5° clockwise. For dual-wavelength mode-locking, the relationship between the fundamental repetition rates difference (Δf) and the peak wavelengths spacing ($\Delta\lambda$) can be calculated as: $\Delta f = L_{\text{total}} D\Delta\lambda / t^2 [20]$, where L_{total} is the total cavity length comprised of ≈ 10.6 m length of passive single-mode fiber and ≈ 1.05 m length of EDF. Based on the fiber parameters, the average group-velocity dispersion of the cavity D_{is} calculated as

$\approx 10.63 \text{ ps} \cdot (\text{nm} \cdot \text{km})^{-1}$, and t_{is} is the roundtrip time of the laser pulse in the cavity. As shown in **Figure 8a**, the measured spectral spacings were 30.488, 30.1905, 29.2804, 29.1229, and 28.7204 nm for PBS positions of 7.0°, 6.5°, 6.0°, 5.5°, and 5.0°. The corresponding repetition rates difference Δf were calculated as 1.147, 1.136, 1.103, 1.096, and 1.081 kHz. Small discrepancies between these calculated values compared to the measured values from the RF spectrum shown in **Figure 8b** could be attributed to the average dispersion parameter value evaluation.

In our proposed experiment, the CSs and QC-NLPs could coexist in the cavity, and these two types of soliton state operations could be switched either by varying the PBS position and/or pump power. To investigate the temporal domain profile of the dual-colored solitons, the output pulse train was recorded at a pump power of 540 mW and for five different PBS positions. As depicted in **Figure 8c**, the two pulse sequences were all split into a random multi-pulse state when the PBS is positioned at 7°. This result indicates that both the pulse-trains in the dual-wavelength mode-locking operation belong to the CSs state. When the

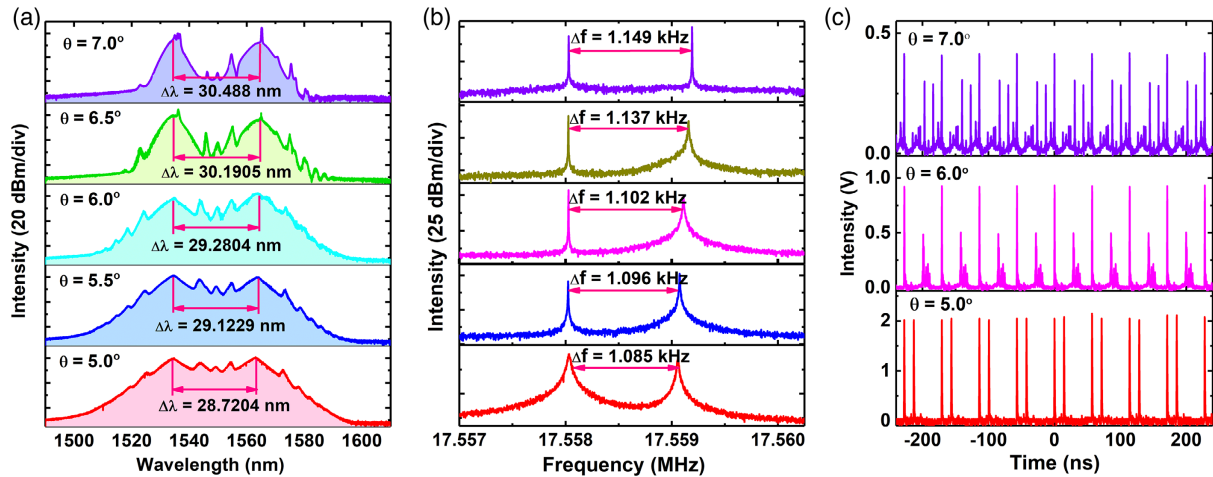


Figure 8. Versatile hybrid dual-wavelength mode-locking operation at different PBS positions: a) output spectra of mode-locked operation; b) corresponding RF spectra; c) monitored output pulse trains at PBS positions of 7.0° , 6.0° , and 5.0° .

PBS is positioned at 6° , one of the pulse sequences was split into a multi-pulse state, while the other maintained its stable single-pulse state. This indicates the dual-wavelength mode-locked output signal comprised of CSs and QC-NLPs states. Positioning PBS at 5° transformed both the pulse-trains to a stable single-pulse state corresponding to dual-QC-NLPs state. During this mode-locking operation, the intensity of the dual-QC-NLPs was higher than that of the other two dual-wavelength mode-locking operations comprised of either two CSs state or one CS state and one QC-NLP state. Thus, easily switchable three different types of hybrid dual-wavelength mode-locking operations are achievable in the proposed single cavity fiber laser, simply through 3D maneuvering of the PBS position.

3.3. Tunable Harmonic Mode-Locking Operation

Due to the cavity birefringence filtering effect, the peak wavelength of mode-locking operation could be tuned by steering

the PBS position. When the PBS position was steered to $\approx 8.2^\circ$ clockwise, a longer wavelength mode-locking was achieved in the fiber laser. The measured output spectrum is shown in Figure 9a. The peak wavelength of the mode-locked signal was 1564.668 nm with a 3-dB spectral bandwidth of 4.83 nm. The output pulse train was stable, as shown in Figure 9b, and the time gap between adjacent pulses was ≈ 56.95 ns. RF spectrum shown in Figure 9c reveals the fundamental repetition rate of the soliton pulses was 17.55749 MHz with a 1-Hz RBW. The measured SNR value of more than 61 dB confirmed the highly stable mode-locking operation. From the temporal profile of the pulse shown in Figure 9d, pulse duration was calculated as ≈ 810.3 fs using a sech^2 profile fit. Similar to the higher order soliton generation in conventional fiber lasers, harmonic mode-locking (HML) was achieved in the proposed fiber laser by increasing the pump power. With the maximum possible pump power of 540 mW, up to the 46th harmonic of the fundamental repetition rate was achieved. The output spectrum is

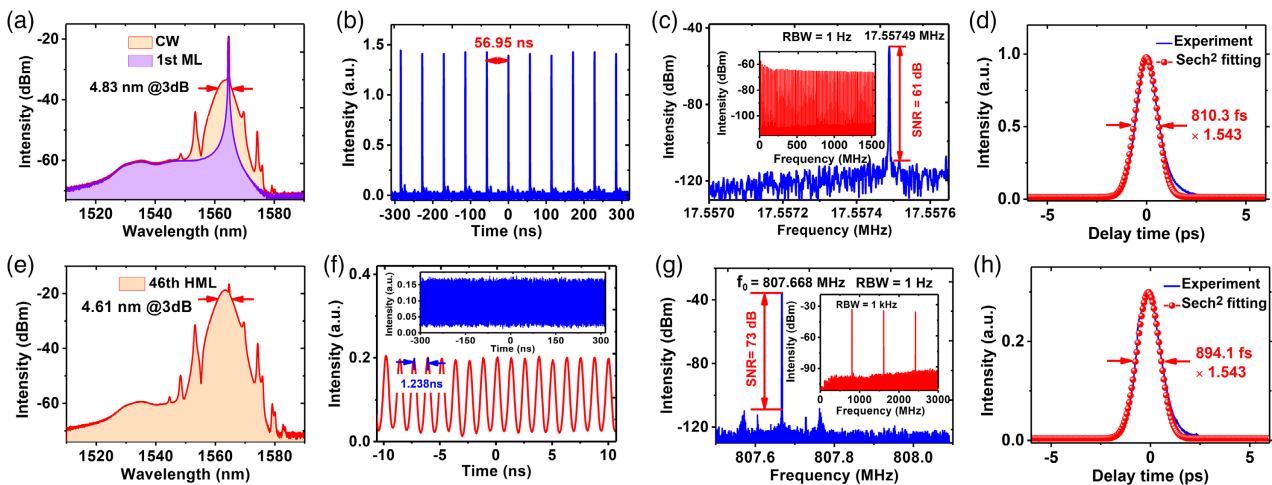


Figure 9. Output characteristics of the 1st and the 46th HML operation: a,e) output spectra; b,f) output pulse trains; c,g) RF spectra; d,h) measured intensity AC traces.

shown in Figure 9e, which depicts the 3-dB spectral bandwidth was 4.61 nm. In the spectral intensity, the CW component was highly subsidized and mostly dominated by the asymmetric Kelly sidebands. Output pulse train shown in Figure 9f, depicts the time gap between adjacent HML pulses was ≈ 1.238 ns, corresponding to 1/46 of the fundamental pulse period. Inset in Figure 9f shows ns scaled oscilloscope trace, which further confirmed the highly stable HML operation. RF spectrum, shown in Figure 9g, indicates the repetition frequency of laser pulses was 807.668 MHz with a 1-Hz RBW, corresponding to the 46th harmonic of the fundamental repetition rate. The dominant-mode distinction ratio of the 46th HML was higher than 70 dB, indicating that the HML operation was highly stable and reliable. Figure 9h depicts the intensity AC trace of the 46th HML pulses. The temporal profile was a single-hump structure with a sech^2 fit pulse duration of ≈ 894.1 fs and no sub-peaks were observed in the pedestal.

As a versatile HML operation, we found that the mode-locking harmonic order could also be selected from 1st to 46th in the cavity by varying the pump power. **Figure 10a** shows the harmonic order as a function of the pump power. As the pump power was increased from 54 to 540 mW, the mode-locking harmonic order in the HML operation gradually hopped from the 3rd harmonic (52.67 MHz) to the 46th harmonic (807.668 MHz). It has to be pointed out that the discrete transitions between different orders of HML operation were observed in a steady stepwise manner. Soliton pulses hopped directly from one order of HML state to the next higher order of HML state without any instabilities or intermediate state in between. Moreover, once a particular order of HML state was established in the cavity, its stable operation was maintained even with small variations around the supplied pump power, resulting in a multi-stable hysteresis characteristic,^[31] as shown in Figure 10a. Similar to lower-to-higher harmonic-order hopping, reverse hopping from higher-to-lower harmonic orders was also achievable in the NPE fiber laser setup by simply decreasing the supplied pump power. Due to the multi-stable hysteresis characteristic associated with the nonlinear cavity, the reverse hopping path is different from the forward hopping path. Another important point is that small adjustments in the PC orientation were exploited to achieve stable higher order HML operation with equal signal amplitude and time spacing. The insets in Figure 10a show the oscilloscope traces of the highly stable 25th and 46th HML operations. Output spectra of different orders of HML operation are displayed in Figure 10b.

Asymmetric Kelly sidebands were observed in the spectra with no obvious interference patterns. A gradual decrease of the CW component intensity was observed during the lower-to-higher harmonic-order hopping of the HML operation, while the 3-dB bandwidth was almost unaltered. The average output power and single pulse energy characteristics with respect to the supplied pump power are shown in Figure 10c. The output power increased monotonically with the pump power with a slope efficiency of 4.5%, and the output power increased from 1.1 to 23.7 mW for the pump power variation from 36 to 540 mW. The behavior of single pulse energy is presented in Figure 10c. A sawtooth kind of variation in the single pulse energy was observed when the cavity dynamics hopped from one HML state to the next higher order HML state. For each order of the HML state, the single pulse energy increased linearly with respect to the supplied pump power. The final single pulse energy of different orders HML operations is also shown in Figure 10c (red circle). In that, a decaying behavior of the final single pulse energy decreasing from 79.96 to 29.37 pJ exhibited a trend of saturation.

4. Conclusion

Through a suitable selection of the polarization state for the intracavity light signal in the proposed NPE fiber laser, we demonstrated a self-starting switchable between different stable and reliable mode-locked soliton states operation. The soliton fiber laser could be easily switched (reversible) between CSs and QC-NLPs states through 3D maneuvering of the PBS position to provide the necessary polarization state for the cavity light signal to achieve desired functionalities. Hybrid dual-wavelength mode-locking operation of a combination of CSs state and QC-NLPs state were also achieved. Monitored very stable functioning of the fiber laser over a period of 150 min for the CSs, QC-NLPs, and HML states confirms the proposed laser system is working very well with long-term stable operation. Versatile dual-wavelength mode-locking operations, including two CSs states, one CSs state and one QC-NLPs state, and two QC-NLPs states, were desirably achieved in the simplified NPE fiber laser through various positioning of the PBS by simple 3D maneuver. To the best of our knowledge, this is the first time ever this type of novel switchable multifunctional hybrid dual-wavelength mode-locking mechanism was demonstrated in a single cavity fiber laser. In addition, up to 807.668 MHz, HML operations were also achieved, corresponding to all the integer

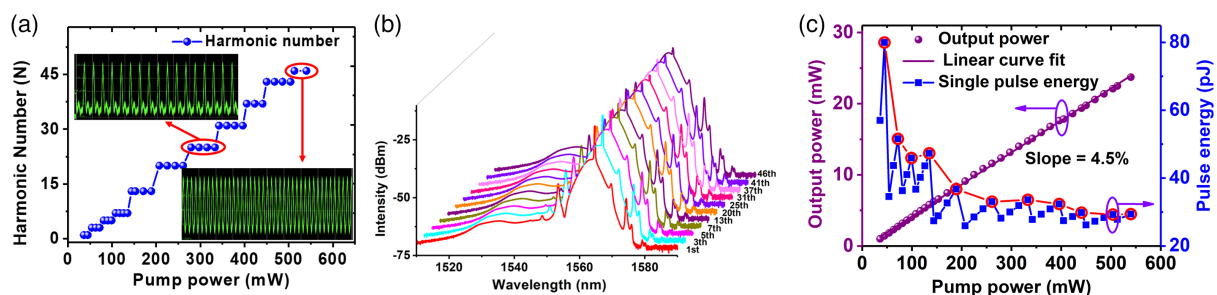


Figure 10. a) Harmonic order as a function of the pump power; b) output spectra of different harmonic orders; c) output power and single pulse energy characteristics with respect to the supplied pump power variation from 36 to 540 mW.

orders up to 46th harmonics of the fundamental repetition rate. For increasing pump power, a sawtooth behavior in the single pulse energy of the harmonics was observed during the HML operations. This self-starting switchable multifunctional mode-locked provides many potential applications including wavelength-division-multiplexing sub-system, optics signal processing, and micromachining.

Acknowledgements

This work was supported by grants from National Natural Science Foundation of China (61805281) and Natural Science Foundation of Guangdong Province, China (2019A1515010732).

Conflict of Interest

The authors declare no conflict of interest.

Data Availability Statement

The data that support the findings of this study are available from the corresponding author upon reasonable request.

Keywords

mode-locked fiber lasers, nonlinear optics, solitons lasers, switchable multifunctional solitons

Received: November 15, 2021

Revised: January 10, 2022

Published online: January 30, 2022

-
- [1] C. Kerse, H. Kalaycıoğlu, P. Elahi, B. Çetin, D. K. Kesim, Ö. Akçaalan, S. Yavaş, M. D. Aşık, B. Öktem, H. Hoogland, R. Holzwarth, F. Ö. Ilday, *Nature* **2016**, 537, 84.
- [2] L. Lundberg, M. Mazur, A. Mirani, B. Foo, J. Schröder, V. Torres-Company, M. Karlsson, P. A. Andrekson, *Nat. Commun.* **2020**, 11, 201.
- [3] J. Capmany, D. Novak, *Nat. Photon.* **2007**, 1, 319.
- [4] Q. Sun, Z. Qin, W. Wu, Y. Lin, C. Chen, S. He, X. Li, Z. Wu, Y. Luo, J. Qu, *Opt. Express* **2018**, 9, 581.
- [5] J. Ye, P. Hannaford, in *Femtosecond Laser Spectroscopy*, Springer, New York **2005**.
- [6] L. E. Nelson, D. J. Jones, K. Tamura, H. A. Haus, E. P. Ippen, *Appl. Phys. B Lasers Opt.* **1997**, 65, 277.
- [7] B. Oktem, C. Ülgüdür, F. Ö. Ilday, *Nat. Photon.* **2010**, 4, 307.
- [8] P. Grelu, N. Akhmediev, *Nat. Photon.* **2012**, 6, 84.
- [9] Z. Wang, K. Nithyanandan, A. Coillet, P. Tchofo-Dinda, P. Grelu, *Phys. Rev. Res.* **2020**, 2, 013101.
- [10] R. Zhou, Q. Li, H. Y. Fu, K. Nakkeeran, *Opt. Lett.* **2021**, 46, 1305.
- [11] L. Orazi, L. Romoli, M. Schmidt, L. Li, *CIRP Ann. Manuf. Techn.* **2021**, 70, 543.
- [12] S. Lei, X. Zhao, X. Yu, A. Hu, S. Vukelic, M. B.G. Jun, H. E. Joe, Y. L. Yao, Y. C. Shin, *J. Manuf. Sci. Eng.* **2020**, 142, 031005.
- [13] J. Liang, L. V. Wang, *Optica* **2018**, 5, 1113.
- [14] I. Coddington, N. Newbury, W. Swann, *Optica* **2016**, 3, 414.
- [15] A. Hishikawa, A. Matsuda, M. Fushitani, *Bull. Chem. Soc. Jpn.* **2020**, 93, 1293.
- [16] N. Nishizawa, *J. Phys. B: At. Mol. Opt. Phys.* **2016**, 49, 182003.
- [17] D. Tang, L. Zhao, G. Xie, L. Qian, *Phys. Rev. A* **2007**, 75, 063810.
- [18] Y. Huang, Z. Hu, H. Cui, Z. Luo, A. Luo, W. Xu, *Opt. Lett.* **2016**, 41, 4056.
- [19] Y. Cui, X. Liu, *Opt. Express* **2013**, 21, 18969.
- [20] B. Liu, Y. Luo, Y. Xiang, X. Xiao, Q. Sun, D. Liu, P. Shum, *Opt. Express* **2018**, 26, 27461.
- [21] R. Li, H. Shi, H. Tian, Y. Li, B. Liu, Y. Song, M. Hu, *Opt. Express* **2018**, 26, 28302.
- [22] Y. Nakajima, Y. Hata, K. Minoshima, *Opt. Express* **2019**, 27, 5931.
- [23] Y. Nakajima, Y. Hata, K. Minoshima, *Opt. Express* **2019**, 27, 14648.
- [24] B. Li, J. Xing, D. Kwon, Y. Xie, N. Prakash, J. Kim, S. Huang, *Optica* **2020**, 7, 961.
- [25] X. Luo, T. Tuan, T. S. Saini, H. P. T. Nguyen, T. Suzuki, Y. Ohishi, *Opt. Express* **2019**, 27, 14635.
- [26] T. Zhu, Z. Wang, D. Wang, F. Yang, L. Li, *Photon. Res.* **2019**, 7, 853.
- [27] L. F. Mollenauer, K. Smith, *Electro. Lett.* **2015**, 51, 351.
- [28] J. Shang, X. Lu, T. Jiang, Y. Lu, S. Yu, *Opt. Lett.* **2018**, 43, 3301.
- [29] W. S. Man, H. Y. Tam, M. S. Demokan, P. K. A. Wai, D. Y. Tang, *J. Opt. Soc. Am. B* **2000**, 17, 28.
- [30] N. Pandit, D. U. Noske, S. M. J. Kelly, J. R. Taylor, *Electron. Lett.* **1992**, 28, 455.
- [31] A. Komarov, H. Leblond, F. Sanchez, *Phys. Rev. A* **2005**, 71, 053809.